JOURNAL OF GUIDANCE, CONTROL, AND DYNAMICS
Vol. 35, No. 6, November–December 2012

Performance Evaluation of an $\mathcal{L}_1$ Adaptive Controller for Wing–Body Rock Suppression

Elisa Capello,* Giorgio Guglieri,† and Daniele Sartori‡
Politecnico di Torino, 10129 Torino, Italy

DOI: 10.2514/1.57595

Wing rock is a rolling motion characterized by self-excited oscillations which appears at high angles of attack in aircraft with highly swept wings. In this paper an analytical model describing this phenomenon is presented for simple wing and wing-fuselage layouts. The parameters of the model were derived through numerical fitting of experimental data. For both cases an $\mathcal{L}_1$ adaptive controller is applied to suppress the wing rock motion for different angles of attack and initial conditions. Adaptation capability is assessed testing the controller action on a model affected by parametric disturbances. The controller can suppress the motion with satisfactory performance for both configurations, even when disturbed.

Nomenclature

A, b, c	=	system matrices
a_i	=	wing rock model parameters
$\hat{a}_i$	=	nondimensional wing rock model parameters
a_{m_1}, a_{m_2}	=	controller parameters
b	=	span, m
$\hat{C}_l$	=	normalized rolling moment coefficient
c_r	=	root chord, m
$D(s)$	=	controller transfer function
$d(t)$	=	nonlinear disturbances
E	=	wing rock motion energy, J
k, k_g	=	controller gains
k_m	=	static feedback gain
l	=	aircraft model C length, m
P	=	solution of algebraic Lyapunov equation
Proj	=	projection operator
Q	=	algebraic Lyapunov equation matrix
Re	=	Reynolds number
t_s	=	reference time, $b/2V$, s
$u(t)$	=	total control
$u_{\text{ad}}(t)$	=	adaptive control
$u_m(t)$	=	feedback control
V	=	airspeed, m/s
α	=	angle of attack, deg
Γ	=	adaptive gain
Δ	=	adaptive signal bound
ζ	=	damping ratio
Θ	=	convex set
$\hat{\theta}(t)$	=	adaptive parameter estimate
Λ	=	sweep angle, deg
$\hat{\sigma}(t)$	=	adaptive disturbance estimate
$\phi(t)$	=	roll angle, deg
ω	=	control effectiveness
ω_l, ω_u	=	lower and upper bounds of control effectiveness
ω_n	=	natural frequency, rad/s
$\hat{\omega}(t)$	=	adaptive controller effectiveness estimate

Received 12 January 2012; revision received 20 March 2012; accepted for publication 21 March 2012.

*Graduated Research Assistant, Dipartimento di Ingegneria Meccanica e Aerospaziale, Corso Duca degli Abruzzi 24; elisa.capello@polito.it.

†Associate Professor, Dipartimento di Ingegneria Meccanica e Aerospaziale, Corso Duca degli Abruzzi 24; giorgio.guglieri@polito.it. Senior Member AIAA.

‡Ph.D. Student, Dipartimento di Ingegneria Meccanica e Aerospaziale, Corso Duca degli Abruzzi 24; daniele.sartori@polito.it.

I. Introduction

THE wing rock phenomenon appears on aircraft characterized by highly swept wing, leading-edge extensions and slender forebody when flying at high angles of attack. It consists in an oscillatory motion about the roll axis which increases in amplitude up to a limit cycle. The appearance of wing rock is due to a nonlinear variation of roll damping with angles of attack and sideslip. Aircraft configurations with slender forebodies are affected by wing rock because of the unsteady interaction between primary forebody vortices and lifting surfaces (leading-edge extensions, wing and stabilizers). It can be encountered by high-speed civil transport and combat aircraft in their flight envelope and, when this occurs, their handling qualities and maneuvering capabilities are seriously degraded. For this reason the suppression of wing rock is a relevant issue. It can be achieved by changing forebody cross section and slenderness or by the adoption of forebody vortex control techniques (boundary-layer suction-blowing and/or movable forebody strakes). The action of these devices must be regulated by an appropriate control law able to handle the complexity of this phenomenon characterized by nonlinearity and parameter uncertainty.

Different techniques have been proposed, such as synergetic optimal controllers [1], fuzzy proportional derivative controllers [2] or variable phase controllers [3]. Singh et al. [4] presented a direct adaptive and neural control for wing rock. With the adaptive control the structure of nonlinearity of the plant is considered, while in the neural control radial basis function neural network is used. Joshi et al. [5] presented a simple rule-based controller to suppress the limit cycle behavior of the wing rock. The rule base is constructed to be linearly separable. A simple neural controller with a single neuron is trained. This method permitted to reduce the computational effort due to parameter tuning. More recently, Liu [6] proposed a new reinforcement adaptive fuzzy control scheme, in which the adaptive channel combined with reinforcement-learning strategy is applied to tune the parameters. Similarly, Cao et al. [7] applied an innovative adaptive and robust $\mathcal{L}_1$ controller.

The purpose of the present paper is the application of an adaptive controller for the suppression of the wing rock phenomenon on a highly swept wing aircraft. Adaptive control theories are chosen because the adaptation channel improves the performance robustness of the feedback path and reduces the tuning effort required to achieve desired closed-loop performance, particularly while operating in the presence of uncertainties and failures. The model considered in this study includes the fuselage and nonlinear uncertainties. The approach presented is similar to [7], where the nonlinearities are

function of the sensor measurement errors (modeled as white noise) and a reduction of the actuator effectiveness is also considered.

A posteriori robust assessment is performed. First, to verify the scalability of the controller, some simulations are carried out considering a wide range of angles of attack and initial conditions. Second, the controller designed on the nominal model is tested on a model with perturbed parameters, so that the steady-state value of the limit cycle reaches a ± 10 deg offset from the nominal case. The proposed approach is simple, robust and stable. As demonstrated in [8–11] $\mathcal{L}_1$ adaptive control is capable of compensating for unexpected, unknown, severe failure events, while delivering predictable performance across the flight envelope without enforcing persistence of excitation, or resorting to gain-scheduling of the control parameters or control reconfiguration. It is shown that $\mathcal{L}_1$ adaptive control architectures have an appropriate structure for the integration of conventional frequency-domain filtering techniques, while providing at the same time a suitable framework for the analysis of the effect of these techniques in the stability and performance characteristics of the closed-loop system.

The remainder of the paper is organized as follows. The wing rock model is discussed in the next section, together with the definition of the experimental parameters. The most relevant features of $\mathcal{L}_1$ adaptive control are then recalled in Sec. III, where the most peculiar aspects related to the present application are discussed with some more details. Some results are then presented and a section of conclusions ends the paper.

II. Wing Rock Model

The nondimensional model describing the motion of the roll angle $\phi(t)$ was derived in [12,13]:

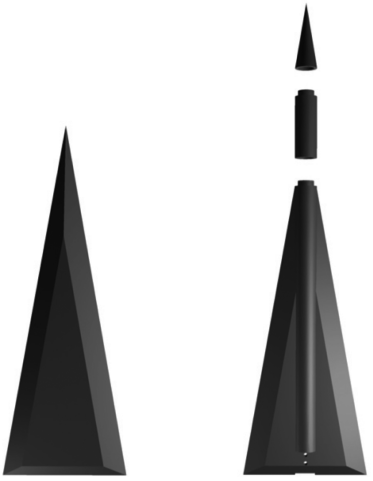

Fig. 1 Configuration models A (left) and C (right) tested in the wind tunnel.

$$\phi''(t) + \hat{a}_0\phi(t) + \hat{a}_1\phi'(t) + \hat{a}_2|\phi'(t)|\phi'(t) + \hat{a}_3\phi^3(t) + \hat{a}_4\phi^2(t)\phi'(t) = \phi''(t) - \hat{C}_l(\phi(t)) = 0 \quad (1)$$

The time derivatives are nondimensional, $\hat{a}_0, \hat{a}_1, \hat{a}_2, \hat{a}_3, \hat{a}_4$ are the parameters relative to the experimental conditions (i.e., angle of attack, airspeed, Reynolds number, and wing characteristics) and $\hat{C}_l(\phi(t))$ is the normalized rolling moment coefficient.

The term $\hat{a}_0\phi(t) + \hat{a}_3\phi^3(t)$ represents the restoring moment, it exhibits a softening of the linear stiffness $\hat{a}_0$ typical of the Duffing equation. For this reason the system is statically divergent for $\phi(t) > \sqrt{-\hat{a}_0/\hat{a}_3}$. The damping coefficient $\hat{a}_1 + \hat{a}_4\phi^2(t)$ is nonlinear and negative for $\phi(t) < \sqrt{-\hat{a}_1/\hat{a}_4}$ (Van der Pol equation). For lower roll angles the system is dynamically unstable, as $\phi(t)$ increases up to the inversion point it becomes stable. The coordinate for this dynamic stability crossover is not coincident with limit cycle amplitude, as the stability of final state occurs when the balance between dissipation and generation of energy E is achieved:

$$E \equiv \oint_\ell \hat{C}_l(\phi(t))\,\mathrm{d}\phi = 0$$

This condition is required for a stable oscillatory limit cycle. Dynamic stability and limit cycle characteristics are also influenced by the additional damping produced by the term $\hat{a}_2|\phi'(t)|\phi'(t)$.

The identification of the parameters $\hat{a}_i$ was performed through least squares approximation of experimental data. Extensive tests were carried out at the D3M low-speed wind tunnel of Politecnico di Torino. As described in [14] different aircraft configurations were considered, among them relevance was given to a plain delta wing (model A) and to a more complex model including wing, forebody and nose tip (model C), see Fig. 1. The wing has the following dimensions: span $b = 0.169$ m, root chord $c_r = 0.479$ m, and sweep $\Lambda = 80$ deg. Total length of model C is $l = 0.568$ m, wing characteristics remain unchanged. The experimental setup scheme is illustrated in Fig. 2. Tests included free to roll conditions with airspeed $V = 30$ m/s ($Re = 950,000$) and angle of attack α ranging from 25 to 45 deg.

As comprehensively explained in [12,13], Eq. (1) is able to accurately describe the behavior of model A. For each α the corresponding limit cycle is reached regardless of the initial conditions up to a release roll angle $\phi_0 = 55$ deg. Simulations of typical roll angle time history and phase plane representation are depicted in Fig. 3. Aerodynamic coefficients $\hat{a}_i$ for all tested angles of attack are listed in Table 1.

Model C shows a different behavior. The unsteady interaction between forebody vortices and lifting surfaces determines more complex wing rock dynamics. The apex of the fuselage generates a pair of vortices which separates from the body along its leeward fore part. These vortices tend to become asymmetric when the angle of attack α exceeds the fuselage apex angle due to ogive surface micro-asymmetries. Unbalanced interference with lifting surfaces determines the typical wing rock oscillatory motion.

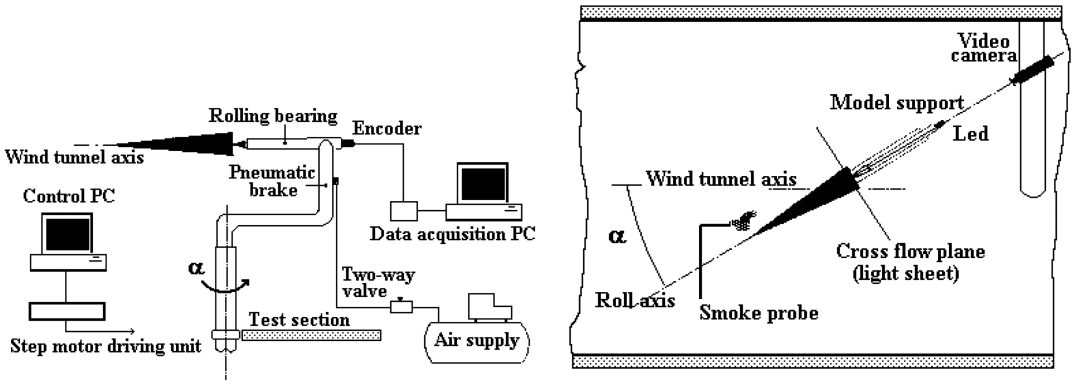

a) Side view b) Top view

Fig. 2 The experimental setup.

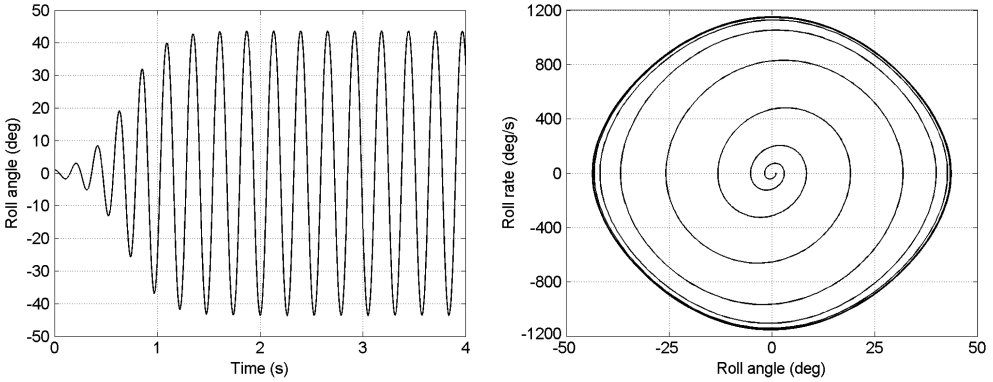

a) Roll angle time history **b) Phase plane representation**

Fig. 3 Free motion simulation for model A: $\alpha = 32.5$ deg; $\phi_0 = 1$ deg; $\dot{\phi}_0 = 0$ deg/s.

Compared to model A, experimental results show that model C needs a longer transient before convergence to a limit cycle. When reached, oscillation amplitudes are smaller as if aerodynamic damping is increased by the fuselage. A singularity is present for $\alpha = 27.5$ deg where wing rock is not triggered. In fact, the model settles to a nonoscillatory steady state caused by the interference between forebody and wing vortices that cancels out the hysteresis of the wing vortex normal displacement. For angles of attack greater than 37.5 deg oscillations amplitude fluctuates or the motion disappears because of the starting of wing vortices breakdown. The type of roll dynamics observed for model C is only partially described as a stable elliptical limit cycle. Occasionally the initial release roll angle ϕ_0 prevents the build up of oscillations, in all other cases when these are triggered the limit cycle is unaffected. A steady-state roll angle offset up to $\Delta\phi = 20$ deg can be reached due to forebody vortices asymmetry, differently steady-state roll angle offset for model A was nonexistent.

Parameters a_i for model C are listed in Table 2. Comparison with Table 1 shows that for $\alpha \leq 35$ deg coefficients representing stiffness ($\hat{a}_0$ and $\hat{a}_3$) are similar. On the contrary, the damping of the systems (identified by $\hat{a}_1$, $\hat{a}_2$, and $\hat{a}_4$) differs substantially because of the presence of fuselage in model C. For $\alpha \geq 35$ deg simulations obtained with the analytical model fail to accurately match experimental results. In fact, forebody vortices alter considerably the shape of the restoring moment term which can no longer be modeled as $\hat{a}_0\phi(t) + \hat{a}_3\phi^3(t)$. The steady-state roll angle offset is filtered by the analytical model, with the exception of $\alpha = 42.5$ deg (a nonoscillatory condition) where it is correctly guessed.

Figure 4 shows roll angle time history and relative phase plane representation for model C when released with angle of attack $\alpha = 32.5$ deg and initial conditions $\phi_0 = 1$ deg, $\dot{\phi}_0 = 0$ deg/s. Comparison with Fig. 3 (where same conditions were applied to model A) highlights the ability of the analytical model to capture the longer build up phase and the reduced amplitude.

Table 1 Aerodynamic coefficients for model A

α	$\hat{a}_{0A}$	$\hat{a}_{1A}$	$\hat{a}_{2A}$	$\hat{a}_{3A}$	$\hat{a}_{4A}$
25.0	0.00543	−0.01426	0.41336	−0.00465	0.00263
27.5	0.00594	−0.01765	0.38793	−0.00487	0.01689
30.0	0.00657	−0.02040	0.38008	−0.00537	0.02596
32.5	0.00732	−0.03104	0.53884	−0.00623	0.04189
35.0	0.00794	−0.03137	0.53455	−0.00751	0.05144
37.5	0.00914	−0.00246	0.00105	−0.01059	0.03736
40.0	0.00902	−0.01881	0.62351	−0.01187	0.06119
42.5	0.00999	−0.03219	1.5118	−0.02862	0.06867
45.0	0.01135	−0.03712	2.4252	−0.08113	0.02935

Table 2 Aerodynamic coefficients for model C

α	$\hat{a}_{0C}$	$\hat{a}_{1C}$	$\hat{a}_{2C}$	$\hat{a}_{3C}$	$\hat{a}_{4C}$
25.0	0.00615	−0.02644	0.82603	−0.00940	0.04934
27.5	0.00310	−0.00057	1.0025	−0.01157	−1.1908
30.0	0.00523	−0.00406	0.09998	−0.00167	−0.00183
32.5	0.00729	−0.01260	0.33063	−0.00506	−0.00378
35.0	0.00591	−0.03024	1.0703	−0.00285	−0.03726
37.5	−0.00406	−0.00588	1.084	0.03646	−0.15374
40.0	0.00574	−0.00771	−0.03172	−0.01095	0.16302
42.5	−0.0040	−0.03261	2.3447	0.13848	0.90542
45.0	−0.00089	−0.02071	0.8361	0.13752	2.8685

III. Controller Design

The design of the $\mathcal{L}_1$ controller follows the procedure described in [15] where an example tackles the wing rock suppression problem. Introducing the reference time $t_s = b/2V$, Eq. (1) becomes

$$\phi'' + \frac{\hat{a}_0}{t_s^2}\phi + \frac{\hat{a}_1}{t_s}\phi' + \hat{a}_2|\phi'|\phi' + \frac{\hat{a}_3}{t_s^2}\phi^3 + \frac{\hat{a}_4}{t_s}\phi^2\phi' = 0$$

including t_s in the $\hat{a}_i$ coefficients it is possible to rewrite the wing rock model equation with dimensional derivatives:

$$\ddot{\phi} + a_0\phi + a_1\dot{\phi} + a_2|\dot{\phi}|\dot{\phi} + a_3\phi^3 + a_4\phi^2\dot{\phi} = 0 \tag{2}$$

Equation (2) is written in state space form, the state is defined as $x = [x_1, x_2]^T = [\phi, \dot{\phi}]^T$. Including disturbances $d(t)$ and the action of the controller $u(t)$ it is possible to obtain

$$\dot{x}(t) = \begin{bmatrix} 0 & 1 \\ -a_0 & -a_1 \end{bmatrix} x(t) + \begin{bmatrix} 0 \\ 1 \end{bmatrix} (-a_2|x_2(t)|x_2(t) - a_3x_1^3(t) - a_4x_1^2(t)x_2(t) + d(t) + \omega u(t)) \tag{3}$$

where $\omega \in \mathbb{R}$ represents the unknown control effectiveness. Calling

$$A = \begin{bmatrix} 0 & 1 \\ -a_0 & -a_1 \end{bmatrix}, \qquad b = \begin{bmatrix} 0 \\ 1 \end{bmatrix},$$

$$f_0(x,t) = (-a_2|x_2(t)|x_2(t) - a_3x_1^3(t) - a_4x_1^2(t)x_2(t) + d(t))$$

Equation (3) can be simply rewritten as

$$\dot{x}(t) = Ax(t) + b(f_0(x,t) + \omega u(t)) \tag{4}$$

The desired output $y(t)$ (roll angle $\phi(t)$) is obtained from the state $x(t)$ through matrix c:

$$y(t) = cx(t) = [1 \quad 0]x(t)$$

The chosen control law $u(t) = u_{\text{ad}}(t) + u_m(t)$ is composed of two terms, a baseline control $u_m(t)$ and an adaptive component $u_{\text{ad}}(t)$. The baseline control

$$u_m(t) = -k_m^T x(t)$$

is designed so that the nominal system of Eq. (4) has desired closed loop dynamics. In fact, substituting $u(t) = -k_m^T x(t) + u_{\text{ad}}(t)$ into Eq. (4), the system becomes

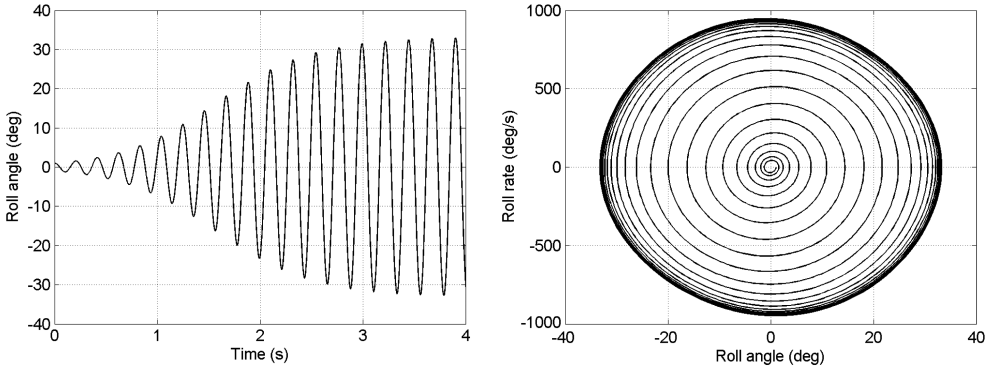

a) Roll angle time history **b) Phase plane representation**

Fig. 4 Free motion simulation for model C: $\alpha = 32.5$ deg; $\phi_0 = 1$ deg; $\dot{\phi}_0 = 0$ deg/s

$$\dot{x}(t) = A_m x(t) + b(f(x,t) + \omega u_{\text{ad}}(t)) \tag{5}$$

where $f(x,t) = f_0(x,t) + (1-\omega)k_m^T x$ and the matrix $A_m = A - bk_m^T$ is Hurwitz with desired poles. Assuming

$$A_m = \begin{bmatrix} 0 & 1 \\ -a_{m1} & -a_{m2} \end{bmatrix}$$

where a_{m1} and a_{m2} are the parameters chosen to define the desired closed loop dynamics, the static feedback gain k_m must be

$$k_m = \begin{bmatrix} a_{m1} - a_0 \\ a_{m2} - a_1 \end{bmatrix}$$

The design of $u_{\text{ad}}(t)$ is more complex and requires an insight of $\mathcal{L}_1$ adaptive control theory. The controller acts so that the error $\tilde{x}$ between the state $x(t)$ of the uncertain nominal plant [in our case described by Eq. (5)] and the state $\hat{x}(t)$ of the predictor is null. The equation of the predictor is

$$\dot{\hat{x}}(t) = A_m \hat{x}(t) + b(\hat{\omega}(t)u_{\text{ad}}(t) + \hat{\theta}(t)\|x(t)\|_\infty + \hat{\sigma}(t))$$

with $\hat{\omega}(t)$, $\hat{\theta}(t)$ and $\hat{\sigma}(t)$ adaptive estimates. These parameters are updated through the adaptation laws

$$\dot{\hat{\theta}}(t) = \Gamma\text{Proj}(\hat{\theta}(t), \quad -\tilde{x}^T(t)Pb\|x(t)\|_\infty), \quad \hat{\theta}(0) = \hat{\theta}_0,$$
$$\dot{\hat{\sigma}}(t) = \Gamma\text{Proj}(\hat{\sigma}(t), \quad -\tilde{x}^T(t)Pb), \quad \hat{\sigma}(0) = \hat{\sigma}_0,$$
$$\dot{\hat{\omega}}(t) = \Gamma\text{Proj}(\hat{\omega}(t), \quad -\tilde{x}^T(t)Pbu_{\text{ad}}(t)), \quad \hat{\omega}(0) = \hat{\omega}_0$$

with $\tilde{x}(t) = \hat{x}(t) - x(t)$, $\Gamma \in \mathbb{R}^+$ is the adaptation gain, $P = P^T > 0$ is the solution of the algebraic Lyapunov equation $A_m^T P + PA_m = -Q$ where $Q = Q^T > 0$ arbitrary. The projection operator Proj (see [15] for its definition) guarantees that adaptive estimates $\hat{\omega}(t)$, $\hat{\theta}(t)$ and $\hat{\sigma}(t)$ are bounded.

The adaptive estimates define $\hat{\eta}(t) = \hat{\omega}(t)u_{\text{ad}}(t) + \hat{\theta}(t)\|x(t)\|_\infty + \hat{\sigma}(t)$, let be $\hat{\eta}(s)$ its Laplace transform. The controller in the frequency domain is defined as

$$u_{\text{ad}}(s) = -kD(s)(\hat{\eta}(s) - k_g r(s)) \tag{6}$$

$u_{\text{ad}}(t)$ is available through inverse Laplace transform of $u_{\text{ad}}(s)$. In Eq. (6) $k_g = -1/(cA_m^{-1}b)$, $r(s)$ is the Laplace transform of the reference signal $r(t)$; the feedback gain $k > 0$ and the strictly-proper transfer function $D(s)$ must be chosen so that $\mathcal{L}_1$ norm condition is verified (see [15] for further details) and to obtain the desired specifications (rise time, settling time, overshoot, etc.). A block scheme of the controller is visible in Fig. 5.

IV. Implementation and Simulation Results

The choice of the elements a_{m_1} and a_{m_2} of A_m is based on the desired closed loop response of the system. The poles of a system defined by such a matrix are obtained solving the quadratic equation

$$s^2 + a_{m_2}s + a_{m_1} = 0 \tag{7}$$

Assuming that the desired response needs to be stable with nonoscillatory characteristics, the desired poles are both chosen real, negative and coincident, $s_{1,2} = -10$. The corresponding quadratic equation is $s^2 + 20s + 100 = 0$, comparing it with Eq. (7) results

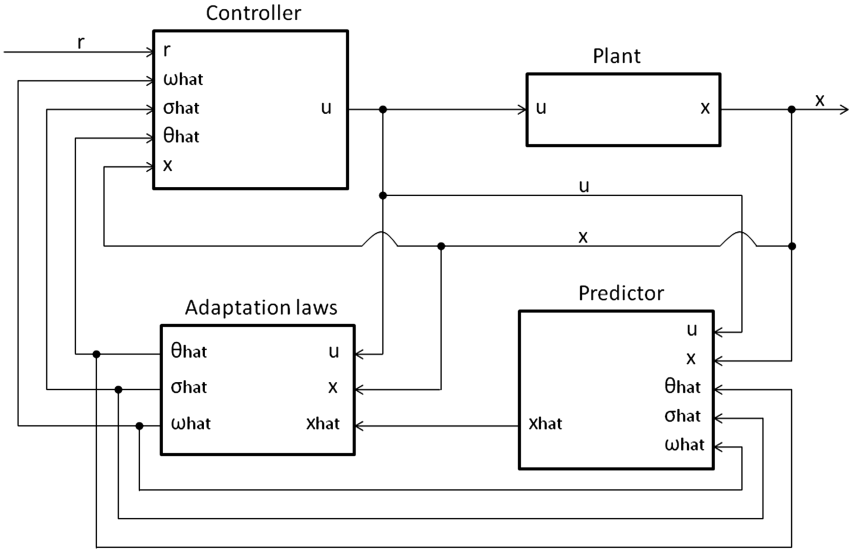

Fig. 5 Block diagram of the $\mathcal{L}_1$ adaptive controller adopted for wing rock suppression.

$a_{m1} = 100$ and $a_{m2} = 20$. Note that the natural frequency and damping of the system are thus $\omega_n = 10$ rad/s and $\zeta = 1$ as

$$A_m = \begin{bmatrix} 0 & 1 \\ -100 & -20 \end{bmatrix} = \begin{bmatrix} 0 & 1 \\ -\omega_n^2 & -2\zeta\omega_n \end{bmatrix}$$

The $\mathcal{L}_1$ adaptive control methodology addresses the problems of traditional adaptive control by providing fast and robust adaptation. The value of the constant $\Gamma = 10,000$ (related to the adaptation) is chosen to guarantee that the steady-state error is minimized. Because of the presence of a low-pass filter in the $\mathcal{L}_1$ controller architecture, high-frequency oscillations are avoided and the system robustness is not reduced. Without loss of generality, it is assumed that

$$\hat{\omega}(t) \in \Omega = [\omega_l, \omega_u], \qquad \hat{\theta}(t) \in \Theta, \qquad |\hat{\sigma}(t)| \leq \Delta$$

where $\omega_u > \omega_l > 0$ are respectively known upper and lower bounds of the control effectiveness, Θ is a compact convex set, and Δ is a known bound for $\hat{\sigma}(t)$. The derivatives of $\hat{\theta}(t)$ and $\hat{\sigma}(t)$ are also considered bounded. The feedback gain k is chosen to guarantee that the state matrix augmented with the feedback channel (closed loop system) is Hurwitz for all $\hat{\omega}(t) \in \Omega$ and $\hat{\theta}(t) \in \Theta$. The proper transfer function $D(s)$ is chosen as in [15]:

$$D(s) = \frac{(s + 500)(s + 0.004)^2}{s(s + 368)(s + 0.00439)^2}$$

A small value, $k = 10$, is taken in order to have a low input signal and so to minimize the required control energy; the control effectiveness ω is assumed to be equal to 0.9, disturbances $d(t)$ are modeled as white noise.

The $\mathcal{L}_1$ adaptive controller model was built in Simulink. Integration is performed through Runge–Kutta method with 0.001 s steps, the controller acts at each integration step.

Simulations include different initial conditions and angles of attack for both models. First a detailed analysis is performed for models A and C at release angle $\alpha = 32.5$ deg and initial conditions $\phi_0 = 10$ deg and $\dot{\phi}_0 = 0$ deg/s. Figure 6 shows the controlled response for models A and C, in both cases the controller effectively sets to zero the roll angle and the roll rate in few seconds. No remarkable difference is observable between the two models, both systems dynamics are dominated by the control law. The nondimensional total control input $u(t)$ is very similar too, as illustrated in Fig. 7. White noise modeled disturbances do not affect the action of the $\mathcal{L}_1$ controller.

Scalability of the controller is tested varying angle of attack and initial conditions for models A and C. Results for $\alpha = 25$, 30, 35, 40 deg and $\phi_0 = 10$ deg, $\dot{\phi}_0 = 0$ deg/s are shown in Fig. 8. No remarkable difference is visible between the two models, the controller is able to suppress wing rock independently of α. Note that this simulation includes the condition $\alpha = 40$ deg where the analytical model for configuration C fails to accurately describe the behavior of the experimental model.

The variation of initial conditions is illustrated in Fig. 9. The reference angle of attack is maintained at $\alpha = 32.5$ deg while the initial roll angle changes between $\phi_0 = -30$ deg and $\phi_0 = 30$ deg, initial roll rate is maintained at $\dot{\phi}_0 = 0$ deg/s. In this interval the motion is perfectly controlled, apparently better for model C. Note that the $\mathcal{L}_1$ controller here developed is not able to suppress wing rock for model A for starting roll angles larger than $\phi_0 = \pm 32$ deg when $\dot{\phi}_0 = 0$ deg/s, divergence occurs. Larger initial roll angles can be achieved only when an opposite initial roll rate is applied to facilitate the controller action; for instance the starting condition $\phi_0 = 33$ deg can be controlled when $\dot{\phi}_0 \leq -32$ deg/s. For model C the acceptable release roll angle is up to $\phi_0 = \pm 35$ deg when $\dot{\phi}_0 = 0$ deg/s. This is motivated by the larger damping effect of the fuselage as previously noticed (see Figs. 3 and 4).

An interesting case for testing the performance of the controller is when model C is released with $\alpha = 42.5$ deg with same initial conditions as before. Figure 10a shows the roll angle behavior characterized by an oscillation offset about the value $\phi = 9.5$ deg.

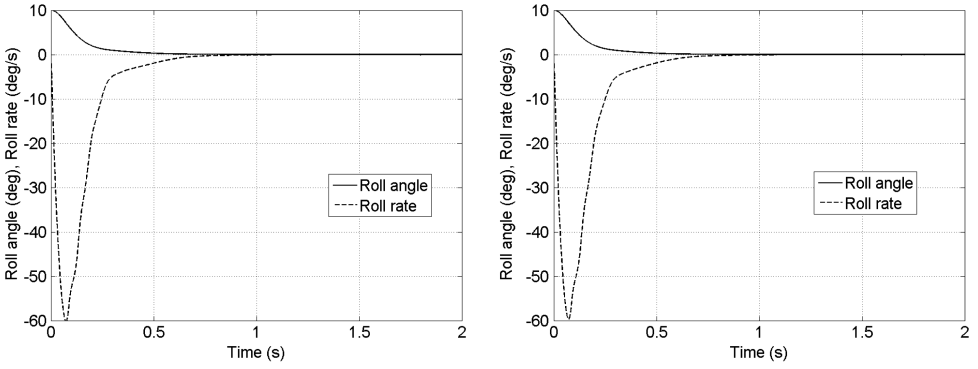

a) Model A **b) Model C**

Fig. 6 Controlled roll angle and roll rate: $\alpha = 32.5$ deg; $\phi_0 = 10$ deg; $\dot{\phi}_0 = 0$ deg/s.

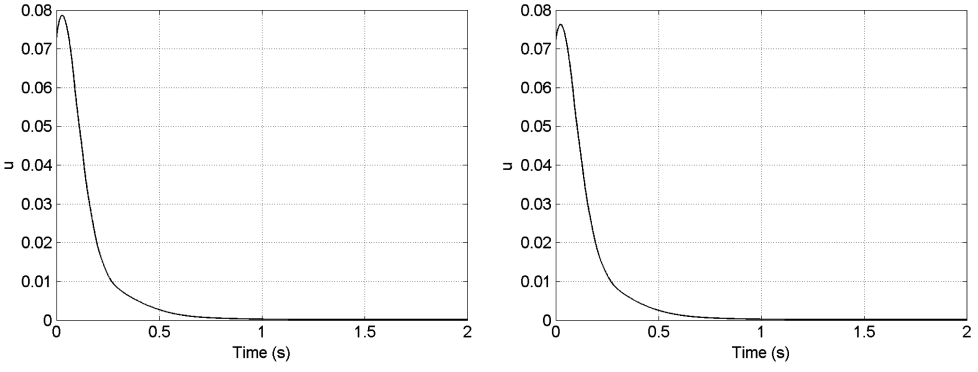

a) Model A **b) Model C**

Fig. 7 Total adimensional control input: $\alpha = 32.5$ deg; $\phi_0 = 10$ deg; $\dot{\phi}_0 = 0$ deg/s.

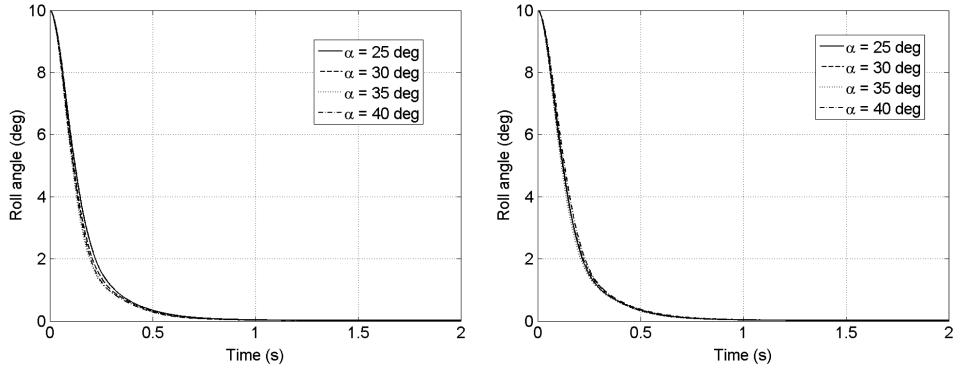

a) Model A **b) Model C**

Fig. 8 Controller action: $\alpha = 25, 30, 35, 40$ deg; $\phi_0 = 10$ deg; $\dot{\phi}_0 = 0$ deg/s.

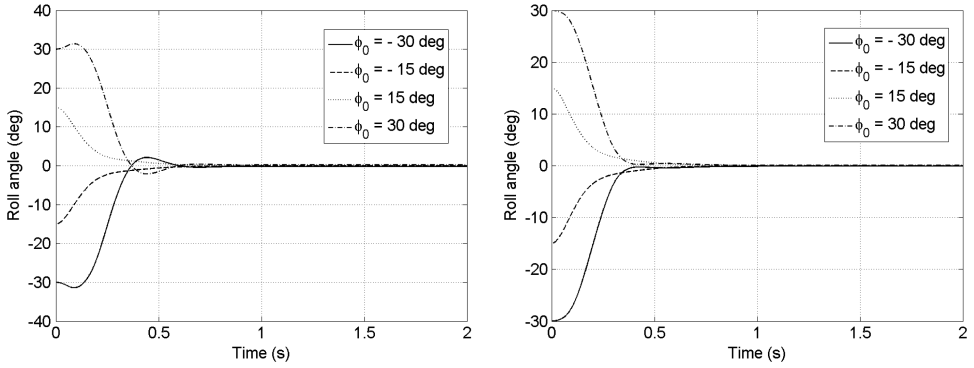

a) Model A **b) Model C**

Fig. 9 Controller action: $\alpha = 32.5$ deg; $\phi_0 = -30, -15, 15, 30$ deg; $\dot{\phi}_0 = 0$ deg/s.

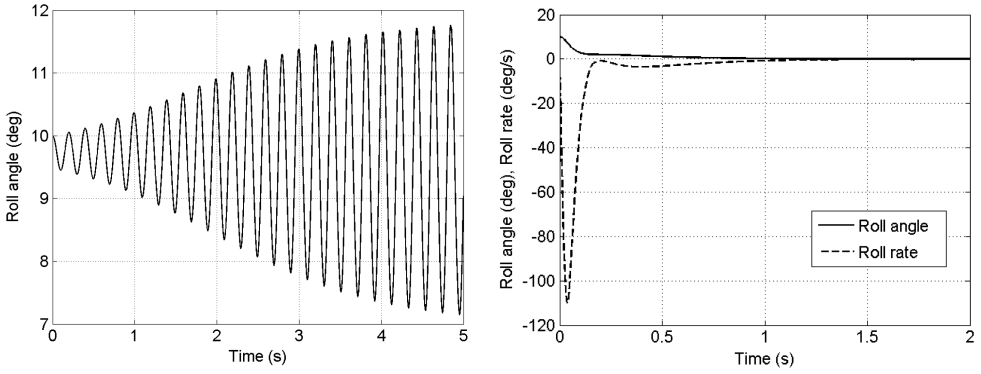

a) Free motion **b) Controlled motion**

Fig. 10 Model C free and controlled motion: $\alpha = 42.5$ deg; $\phi_0 = 10$ deg; $\dot{\phi}_0 = 0$ deg/s.

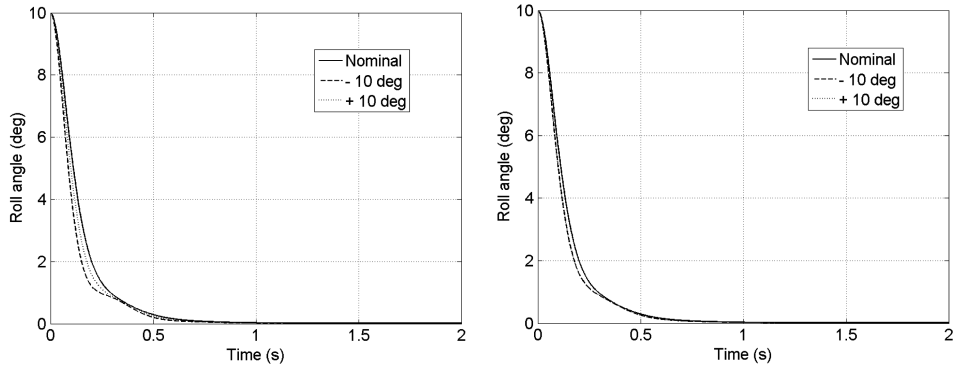

a) Perturbation of a_0 **b) Perturbation of a_1**

Fig. 11 Model C controlled motion with parameters perturbation: $\alpha = 32.5$ deg; $\phi_0 = 10$ deg; $\dot{\phi}_0 = 0$ deg/s.

Even in this case the controller effectively cancels out roll oscillations in few seconds, with an action slower but yet similar to the previous cases.

One characteristic of wing rock motion is the presence of aerodynamic asymmetries, couplings and wing–body vortex interactions which can hardly be modeled, even fitting experimental data. The parameters $\hat{a}_i$ of Eq. (1) are estimated from tests and contain a level of uncertainty ($\Delta\phi(t) = \pm 10$ deg) which can alter the performance of the controller. The capability of the controller to handle these variations is tested perturbating separately coefficients $\hat{a}_0$ and $\hat{a}_1$. The amount of perturbation guarantees that the steady-state angular value of the limit cycle in free motion reaches a ± 10 deg offset from the nominal case. In Eq. (1) the parameter $\hat{a}_0$ has the meaning of linear stiffness in the restoring moment $\hat{a}_0\phi(t) + \hat{a}_3\phi^3(t)$ and $\hat{a}_1$ represents a constant damping parameter of the overall damping coefficient $\hat{a}_1 + \hat{a}_4\phi^2(t)$. The analysis is performed for model C for a release angle $\alpha = 32.5$ deg and initial conditions $\phi_0 = 10$ deg, $\dot{\phi}_0 = 0$ deg/s. In Fig. 11 the effectiveness of the controller action is validated with the presence of perturbation, in particular a smaller sensitivity is shown with respect to parameter $\hat{a}_1$.

V. Conclusions

This paper describes the application of an $\mathcal{L}_1$ adaptive controller to suppress the wing rock phenomenon. Both an isolated highly swept wing and a complete configuration with fuselage and forebody are analyzed for different angles of attack and initial conditions. Disturbances and changes in the state parameters are included to validate the robustness of the controller to adapt to the level of uncertainty that characterizes wing–body rock modeling. In each of the simulated cases the controller effectively cancels oscillations in a short time with a limited amount of energy input. No remarkable difference in performance is observable among the different scenarios, suggesting that the design is able to handle the effect of aircraft configuration with adequate robustness.

Acknowledgments

The authors thank Naira Hovakimyan and her group at the University of Illinois at Urbana–Champaign for sharing experience and knowledge on the $\mathcal{L}_1$ controller theory and implementation.

References

[1] Nusawardhana, A., Zak, S. H., and Crossley, W. A., "Nonlinear Synergetic Optimal Controllers," *Journal of Guidance, Control, and Dynamics*, Vol. 30, No. 4, July–Aug. 2007, pp. 1134–1148. doi:10.2514/1.27829

[2] Liu, Z. L., Su, C.-Y., and Svoboda, J., "Control of Wing Rock Using Fuzzy PD Controller," *The 12th IEEE International Conference on Fuzzy Systems*, Vol. 1, May 2003, pp. 414–419.

[3] Liu, Z. L., Su, C.-Y., and Svoboda, J., "Variable Phase Control of Wing Rock," *Aerospace Science and Technology*, Vol. 10, No. 1, Jan. 2006, pp. 27–35. doi:10.1016/j.ast.2004.11.002

[4] Singh, S. N., Yim, W., and Wells, W. R., "Direct Adaptive and Neural Control of Wing-Rock Motion of Slender Delta Wings", *Journal of Guidance, Control, and Dynamics*, Vol. 18, No. 1, Jan.–Feb. 1995, pp. 25–30. doi:10.2514/3.56652

[5] Joshi, S. V., Sreenatha, A. G., and Chandrasekhar, J., "Suppression of Wing Rock of Slender Delta Wings Using a Single Neuron Controller," *IEEE Transactions on Control Systems Technology*, Vol. 6, No. 5, Sept. 1998, pp. 671–677. doi:10.1109/87.709502

[6] Liu, Z. L., "Reinforcement Adaptive Fuzzy Control of Wing Rock Phenomena," *IEE Proceedings D: Control Theory Applications*, Vol. 152, No. 6, Nov. 2005, pp. 615–620. doi:10.1049/ip-cta:20045072

[7] Cao, C., Hovakimyan, N., and Lavretsky, E., "Application of $\mathcal{L}_1$ Adaptive Controller to Wing-Rock," AIAA Guidance, Navigation, and Control Conference and Exhibit, AIAA Paper 2006-6426, Keystone, CO, Aug. 2006.

[8] Patel, V. V., Cao, C., Hovakimyan, N., Wise, K. A., and Lavretsky, E., "$\mathcal{L}_1$ Adaptive Controller for Tailless Unstable Aircraft in the Presence of Unknown Actuator Failures", *International Journal of Control*, Vol. 82, No. 4, April 2009, pp. 705–720. doi:10.1080/00207170802225955

[9] Dobrokhodov, V., Kitsios, I., Kaminer, I., Jones, K. D., Xargay, E., Hovakimyan, N., Cao, C., Lizàrraga, M. I., and Gregory, I. M., "Flight Validation of Metrics Driven $\mathcal{L}_1$ Adaptive Control," AIAA Guidance, Navigation, and Control Conference, AIAA Paper 2008-6987, Honolulu, HI, Aug. 2008.

[10] Gregory, I. M., Cao, C., Xargay, E., Hovakimyan, N., and Zou, X., "$\mathcal{L}_1$ Adaptive Control Design for NASA AirSTAR Flight Test Vehicle," AIAA Guidance, Navigation, and Control Conference, AIAA Paper 2009-5738, Chicago, IL, Aug. 2009.

[11] Gregory, I. M., Xargay, E., Cao, C., and Hovakimyan, N., "Flight Test of $\mathcal{L}_1$ Adaptive Controller on the NASA AirSTAR Flight Test Vehicle," AIAA Guidance, Navigation, and Control Conference, AIAA Paper 2010-8015, Toronto, Aug. 2010.

[12] Guglieri, G., and Quagliotti, F. B., "Experimental Observation and Discussion of the Wing Rock Phenomenon," *Aerospace Science and Technology*, Vol. 1, No. 2, Feb. 1997, pp. 111–123. doi:10.1016/S1270-9638(97)90041-9

[13] Guglieri, G., and Quagliotti, F. B., "Analytical and Experimental Analysis of Wing Rock," *Nonlinear Dynamics*, Vol. 24, No. 2, 2001, pp. 129–146. doi:10.1023/A:1008328528873

[14] Guglieri, G., "A Comprehensive Analysis of Wing Rock Dynamics for Slender Delta Wing Configurations," *Nonlinear Dynamics*, Vol. 67, No. 10, 2012, pp. 1559–1575. doi:0.1007/s11071-012-0369-3

[15] Hovakimyan, N., and Cao, C., $\mathcal{L}_1$ *Adaptive Control Theory*, Society for Industrial and Applied Mathematics, Philadelphia, 2010, pp. 80–94.

K. Wise
Associate Editor